minerals

MDPI

Article

Metasomatic to Hydrothermal Genesis of Natural Calcium Silicate Hydrates (C-S-H): Evidence from Lessini Mountains, Veneto Volcanic Province, Italy

Michele Mattioli [1,*], Matteo Giordani [1] and Franco Filippi [2]

[1] Department of Pure and Applied Sciences, University of Urbino Carlo Bo, 61029 Urbino, Italy; matteo.giordani@uniurb.it
[2] Independent Researcher, Strada Vicinale Monte Crocetta 33, 36100 Vicenza, Italy; filippifranco43@gmail.com
* Correspondence: michele.mattioli@uniurb.it

Abstract: We report the occurrence of natural calcium silicate hydrates (C-S-H) from the Grolla quarry in the Lessini Mountains of Northern Italy. These minerals are formed by basic and ultrabasic magma interacting with carbonate rocks. The mineral assemblage includes thaumasite, xonotlite, tobermorite, and plombierite, often intergrown with other silicates, as well as minor amounts of carbonates and sulfates. Common zeolites in this area include chabazite, phillipsite/harmotome, natrolite, and thomsonite. Although less abundant, these zeolites are typically associated with calcite, fluoroapophyllite, and barite. The Grolla quarry outcrop allows for the study of the in situ complex crystalline overgrowths and specific crystal chemistry of rare natural mineral phases, such as C-S-H minerals, formed under metasomatic to hydrothermal conditions.

Keywords: C-S-H; tobermorite; plombierite; xonotlite; thaumasite; zeolites; Grolla quarry

Academic Editors: Teresa Pereira da Silva, Daniel P. S. De Oliveira and João Pedro Veiga

Received: 23 November 2024
Revised: 17 December 2024
Accepted: 23 December 2024
Published: 28 December 2024

Citation: Mattioli, M.; Giordani, M.; Filippi, F. Metasomatic to Hydrothermal Genesis of Natural Calcium Silicate Hydrates (C-S-H): Evidence from Lessini Mountains, Veneto Volcanic Province, Italy. *Minerals* **2025**, *15*, 26. https://doi.org/10.3390/min15010026

1. Introduction

Calcium silicate hydrate minerals (C-S-H, the dashes denoting their versatile stoichiometry) [1] are natural and synthetic phases that are of great scientific and technological interest. In particular, C-S-H (according to cement shorthand, C = CaO, S = SiO_2 and H = H_2O) are the main binding phases in many artificial materials, such as aerated concrete (with or without additives), mortars and cement paste, making up 60%–70% of a fully hydrated paste. Due to their critical role in the safety of building structures and construction, C-S-H minerals have been extensively studied, as reflected in the abundant literature [2–6]. C-S-H minerals have a variable composition, are often X-ray amorphous, and can include aluminum and other guest ions. Aluminum incorporation likely affects the chemical and mechanical properties of C-S-H [7]. Improving the strength and durability of hydrated cement—by addressing factors like porosity, creep, shrinkage, and aging—requires a deep understanding of the C-S-H structure at the crystalline level and the atomic scale up to 100 nm [8,9].

Although C-S-H crystalline phases are the main components of artificial materials such as cement, they are rare as minerals of natural origin, especially due to their particular environment and condition of formation. Only a small number of restricted geological environments are known for their natural C-S-H phases, and the main occurrences come from ultrabasic rocks associated with ophiolite complexes involved in low-temperature serpentinization process, or hornfels (contact metamorphic zones with high temperature and low pressure) around igneous intrusions in limestones and calcareous shales [10–12].

During the metasomatic processes that take place in these conditions, significant quantities of volatiles (especially water) can be mobilized, inducing the formation of C-S-H phases such as xonotlite, tobermorite, plombierite, afwillite, hillebrandite, and scawtite [13–15]. This family of minerals is particularly interesting for their various structural arrangements and the peculiar transformation processes in which they are involved (e.g., dehydration). For example, the natural mineral tobermorite is often used as a model to study the molecular structure of C-S-H [16]. Investigating the long-term alteration and carbonation (10s or 100s of thousands of years) of these minerals also makes it very important to simulate man-made Portland cement alteration and, for example, to the sealing performance of well cement systems [4,12]. Moreover, C-S-H minerals are able to exchange cations and have potential applications in waste disposal [17]. Therefore, obtaining data on the crystallization of C-S-H under natural conditions and its transformations is particularly important for understanding cement mixtures' hardening and durability mechanisms.

In this study, different samples of C-S-H phases naturally crystallized in the Lessini Mountains, Northern Italy, were mineralogically and chemically characterized to describe the mineralization within a rare and unusual geological context. Various methodologies were employed, including binocular microscope observations, environmental scanning electron microscope (ESEM) observations, chemical composition analysis (SEM-EDS), and X-ray powder diffraction (XRPD) analysis. The origins of the natural C-S-H phases and potential toxicological aspects are also discussed.

2. Geological Background

The Veneto Volcanic Province covers about 2000 square kilometers in Northern Italy (Figure 1). Due to tectonic tension in the South Alpine foreland, volcanic activity began in the Tertiary period, mostly underwater [18]. Volcanic eruptions happened in bursts from the Late Paleocene to the Miocene, each lasting briefly and separated by inactive phases with shallow-water carbonate deposits [19–21]. This volcanic area has four main districts: the Lessini Mountains, Marostica Hills, Berici Hills, and Euganei Hills. The main rock types include volcaniclastic rocks, hyaloclastites, pillow lavas, and lava flows of mafic to ultramafic composition. In the Euganei Hills, acidic rocks like rhyolite are also found.

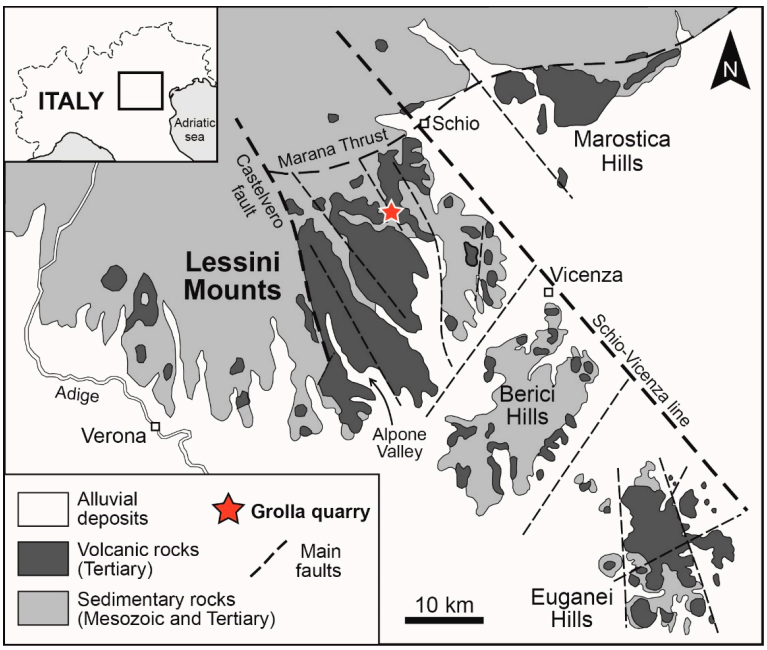

Figure 1. Simplified geological map of the Veneto Volcanic Province highlighting the Lessini Mountains and the location of the Grolla quarry.

The Lessini Mountains stretch from Mt. Baldo in the west to the Schio-Vicenza tectonic line in the east, within a north-northwest-oriented extensional structure called the Alpone-Agno graben. The western fault defines the Castelvero boundary, which was key in shaping the region's environment from the Late Paleocene to the Middle Eocene. This fault separated a sediment-dominated western area with thin volcanic layers from an eastern area rich in volcanic rocks. With layers up to 400 m thick, the Lessini Mountains form the largest volcanic sequence in the Veneto Volcanic Province [20]. The area's volcanism includes mainly tuffs and lava flows, with column-like eruptive necks, hyaloclastites, and pillow lavas. Common rock types are basanite and alkali olivine basalt, with smaller amounts of transitional basalts, nephelinite, hawaiites, trachy-basalt, and basaltic andesites. Studies indicate that the magmatism here has within-plate characteristics, likely forming in a tensional setting as a foreland response to the Alpine orogeny [22–24].

The volcanic rocks of the Lessini Mountains are often extensively altered by intense hydrothermal activity. This process results in significant secondary mineralization, filling numerous cavities and vesicles within the volcanic rocks and forming new mineral phases [25]. Among these, zeolites are the most abundant group, including minerals such as analcime, chabazite, phillipsite, harmotome, and gmelinite. Rare zeolites with distinctive features, such as willhendersonite and yugawaralite, have also been identified in the area [25–27]. Additionally, in recent years, other fibrous zeolites (including carcinogenic erionite, and potentially toxic offretite, mordenite, and ferrierite) have been discovered in several localities of the Lessini Mountains, highlighting their particular importance in toxicological research [28–33].

A rare but significant type of mineralization in the Lessini area is associated with thermometamorphism, a process occurring at very high temperatures and low pressures. This phenomenon affects sedimentary rocks near volcanic bodies, creating a contact zone (or aureole) around the magma. New minerals often form within this aureole, influenced by the type of rocks present, the chemical composition of circulating fluids, and the prevailing P-T conditions. A distinctive form of thermometamorphism occurs when basic magmas, hydrothermally altered volcanic rocks, and carbonate rocks interact. During metasomatism, chemical exchange between rocks releases volatile substances, mainly water. This likely leads to the formation of hydrated calcium silicates like xonotlite, tobermorite, and plombierite, making the Grolla quarry a globally important site for studying these minerals.

3. Materials and Methods

3.1. Materials

All the samples analyzed in this study were collected from the Grolla quarry in Cornedo Vicentino (VI), Lessini Mountains, Italy. Grolla quarry is an active site that produces calcareous materials for construction, prized for their excellent technical and mechanical properties. Large veins and volcanic conduits were uncovered during quarrying operations, cutting through a sequence of carbonate sedimentary rocks. Tertiary basic magmatism led to the formation of abundant crystals in the contact zones between hydrothermally altered basic rocks and calcareous rocks. These crystals range in size from macroscopic (>1 cm) to microscopic (<<1 mm) and are found growing in veins, cavities, and vesicles within deeply metasomatized rocks. The cavities and vesicles vary from millimeters to centimeters and may be fully or partially filled with secondary minerals. In some cases, a single mineral species occupies the space, while in others, multiple species coexist in paragenetic associations. Over 150 samples were collected from various quarry sectors, with 20 selected for detailed investigation to represent the diversity observed in the field.

3.2. Optical and Scanning Electron Microscopy

Observations of the morphology and physical properties were conducted directly on the cavities and vesicles using a Leica Wild Mod. M10 binocular optical microscope at the Department of Pure and Applied Sciences, University od Urbino, Italy, with IntraLux 5000-1 fiber optic illumination, and a DCM-510 Digital image acquisition system.

Small-scale morphological observations were conducted using an environmental scanning electron microscope (ESEM) FEI Quanta 200 FEG, at the Department of Pure and Applied Sciences, University od Urbino, Italy, equipped with an energy-dispersive X-ray spectrometer (EDS) for qualitative microchemical analysis. The settings included a 25 kV accelerating voltage, adjustable beam diameter, a working distance of 10–12 mm, and a tilt angle of 0°. The ESEM operated in low vacuum mode, with the chamber pressure between 0.80 and 0.90 mbar. Images were captured using a single-shot detector (SSD) or an Everhart–Thornley secondary electron detector (ETD). Microchemical analysis was conducted using a JEOL 6400 SEM at the University of Parma, Italy, following the methods outlined in the references [34,35]. The operating conditions were voltage 15 kV, beam current 1.2 nA, and counting time 100 s. The errors are 2%–5% for the major elements and 5%–10% for the minor ones. Compositions of elements, oxides, and silicates were used as standards.

3.3. X-Ray Powder Diffraction

Pure crystals were carefully selected from each sample under a binocular microscope, then disaggregated, finely ground in an agate mortar, and placed in a 0.7 mm side-opened aluminum sample holder. X-ray powder diffraction (XRPD) data were collected using a Philips X'Change PW1830 powder diffractometer at the Department of Pure and Applied Sciences, University od Urbino, Italy, set to 35 kV accelerating voltage and 30 mA beam current, with CuKα radiation (λ = 1.54506 Å). Measurements were made in Bragg–Brentano geometry from 2° to 65° at 2θ, with a 0.01° step size and 2.5 s per step to obtain high-intensity patterns. The diffractometer used a 1° maximum divergence compensating slit, a 0.2 mm receiving slit, and a graphite crystal monochromator. Semi-quantitative XRPD analysis was conducted using X'Pert Quantify and X'Pert HighScore Plus software, version 5.2 release, with quartz as the internal calibration standard. Peak width variations were minimal (within $\pm$2% of the average value), and each sample was measured three times. Detailed X-ray diffraction analyses with extended exposure times (up to 24 h) were performed for each sample to determine the mineralogical composition, assess the separated crystals' quality, and rule out the presence of impurities.

4. Results and Discussion

A summary of the investigated samples and their related mineralogical composition is reported in Table 1. The minerals identified at the Grolla quarry are predominantly silicates, with smaller amounts of carbonates and sulfates. The most common silicates belong to the zeolite group, including chabazite, phillipsite/harmotome, natrolite, and thomsonite. Though generally minor, these zeolites are typically associated with varying amounts of calcite, fluoroapophyllite, and barite. This mineral assemblage is consistent with similar occurrences reported from other parts of the Lessini Mountains [25]. However, unlike other mineralized areas in the Lessini Mountains, the Grolla quarry uniquely yields calcium silicate hydrate minerals (C-S-H) alongside the previously mentioned minerals. Specifically, we identified thomsonite, xonotlite, tobermorite, and plombierite (Table 1). The powder XRD patterns of these C-S-H natural phases are shown in Figure 2. The narrow peaks indicate high crystallinity. Table 2 lists their chemical compositions, which match the ideal stoichiometry. Backscattered electron imaging during ESEM analysis showed

no unusual grains or secondary phases in the investigated samples. The C-S-H minerals described below were positively identified using X-ray powder diffraction, optical data, and chemical microanalyses. While stoichiometries and optical data resembling other phases (e.g., afwillite, scawtite, jennite, clinotobermorite) were obtained, definitive identification was not possible due to the absence of clear X-ray data.

Table 1. Summary of the investigated samples from Grolla quarry and their related mineralogical composition, identified through optical microscope, environmental scanning electron microscope (ESEM), and X-ray powder diffraction (XRPD) analyses. Calcium silicate hydrates are in **bold**.

Sample	Mineralogical Composition
CG1	Phillipsite, Thomsonite, Chabazite, Calcite
CG2	Barite, Chabazite
CG3	Chabazite
CG4	**Xonotlite**, Apofillite, Chabazite, Calcite
CG5	Apofillite, Natrolite, Calcite
CG6	Thomsonite
CG7	**Xonotlite**, Chabazite, Thomsonite
CG8	Chabazite, Phillipsite/Armotomo
CG9	Chabazite, Apophyllite, Calcite
CG11	**Thaumasite**, **Xonotlite**
CG12	Thomsonite, Calcite
CG13	**Xonotlite**, Calcite
CG14	**Tobermorite**, **Plombierite**, **Xonotlite**, Calcite
CG16	Thomsonite, Chabazite, Calcite
CG17	**Xonotlite**, **Tobermorite**, Fluorapophyllite
CG18	Thomsonite, Calcite
CG19	**Tobermorite**, **Plombierite**, Thomsonite, Calcite
CG20	**Thaumasite**, Fluorapophyllite, Chabazite, Calcite
CG21	Natrolite, Calcite
CG30	Chabazite
CG39	**Tobermorite**, **Plombierite**, Calcite

4.1. Xonotlite $Ca_6Si_6O_{17}(OH)_2$

Xonotlite was first identified by Rammelsberg in 1866 in carbonate rocks that had undergone contact metamorphism with magma in Tetela de Xonotla, Mexico (whence the mineral is given its name) [36]. Since then, although it is a rare mineral, xonotlite has been discovered to fill veins and cavities in heat-altered rocks, and less commonly due to metasomatic reactions in rodingites [37]. Xonotlite has a monoclinic crystal structure, typically forming thin, needle-like (acicular) or fibrous crystals a few millimeters in size. Its structure consists of chains of tetrahedra alternating with calcium–oxygen layers [38]. These layers contain calcium ions in two coordination types: seven-fold (CaO_7) and octahedral (CaO_6) [39]. This arrangement allows xonotlite to exist in at least six structural variations (four ordered and two disordered forms) or polytypes [40,41].

Xonotlite is common in the Grolla quarry and appears in various forms (Figure 3a,b). It often forms very thin, needle-like crystals grouped into silky, fibrous clusters. These are generally white inside but may appear white to pink on the surface. Another frequent type is small, transparent needle-like crystals sometimes found in small bundles. Xonotlite also forms isolated, silky-looking spheroidal clusters with glassy crystals. The crystals sometimes grow in parallel, forming fibrous white layers that follow the rock's surface. In other cases, the crystals are so fine that they appear as white, earthy coatings visible only under a microscope. Under an electron microscope, xonotlite crystals are always thin

and fibrous, ranging from a few microns to hundreds of microns in length, with diameters smaller than one micron (Figure 4). Larger crystals sometimes show their monoclinic shape, dominated by prism-like features. In samples from the Grolla quarry, xonotlite is often found in aggregates, alongside large fluoroapophyllite crystals and small calcite rhombohedrons. In all investigated samples, xonotlite always forms on the surface of other minerals and seems to develop in the final stages of crystallization.

Table 2. Representative chemical composition of the natural C-S-H minerals from the Grolla quarry. H_2O has been calculated by difference.

	Thaumasite								**Xonotlite**					
	CG11-01	CG11-02	CG11-03	CG20-01	CG20-02	CG20-06	CG20-07	CG20-08	CG17-01	CG17-02	CG17-03	CG17-04	CG17-08	CG17-09
SiO_2	9.85	9.81	10.02	9.98	9.75	9.91	9.88	10.05	50.15	49.61	49.24	50.44	50.25	49.98
Al_2O_3	bdl	bdl	bdl	bdl	bdl	bdl	bdl	bdl	0.05	bdl	0.04	0.02	0.05	0.02
FeO_{tot}	0.1	0.11	0.23	0.1	0.25	0.2	0.12	0.2	0.07	0.21	0.04	0.11	0.15	0.05
MnO	0.04	0.02	bdl	0.04	bdl	bdl	bdl	0.05	bdl	bdl	bdl	bdl	bdl	bdl
MgO	bdl	bdl	bdl	bdl	bdl	bdl	bdl		0.02	0.12	bdl	0.22	0.21	0.15
CaO	26.95	26.94	26.55	26.78	26.81	26.88	26.64	26.88	47.45	46.66	47.17	48.13	47.74	47.61
P_2O_5	0.42	0.41	0.55	0.38	0.42	0.46	0.35	0.44	bdl	bdl	bdl	bdl	bdl	bdl
SO_3	12.27	12.29	12.21	12.43	12.77	12.35	12.21	12.85	bdl	bdl	bdl	bdl	bdl	bdl
CO_2	7.1	7.51	6.85	7.88	7.41	7.15	6.55	6.97	bdl	bdl	bdl	bdl	bdl	bdl
(F, Cl)	0.25	0.28	0.3	0.18	0.22	0.24	0.35	0.21	bdl	bdl	bdl	bdl	bdl	bdl
H_2O	43.02	42.63	43.29	42.23	42.37	42.81	43.9	42.35	2.31	3.4	3.55	1.1	1.65	2.21
Total	100	100	100	100	100	100	100	100	100	100	100	100	100	100
	Tobermorite											**Plombierite**		
	CG19-01	CG19-02	CG19-03	CG19-06	CG14-01	CG14-02	CG14-04	CG14-05	CG14-09	CG14-10	CG14-11	CG39-01	CG39-02	CG39-03
SiO_2	45.12	45.31	45.22	45.19	45.41	44.53	45.68	44.84	43.81	44.12	43.05	41.91	41.76	41.05
TiO_2	bdl	0.02	bdl	0.02	bdl	bdl	bdl	bdl	bdl	bdl	bdl	bdl	bdl	bdl
Al_2O_3	0.31	0.39	0.41	0.38	0.31	0.25	0.28	0.26	0.15	0.11	0.23	1.05	1.14	1.05
CaO	35.11	34.22	34.06	34.52	35.15	34.18	34.55	34.61	30.47	31.09	32.6	33.12	33.17	33.84
H_2O	19.46	20.06	20.31	19.89	19.13	21.04	19.49	20.29	25.57	24.68	24.12	23.92	23.93	24.06
Total	100	100	100	100	100	100	100	100	100	100	100	100	100	100

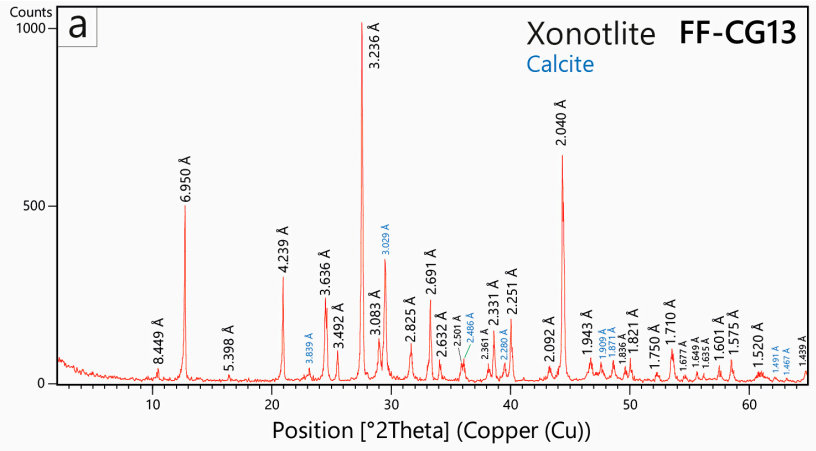

Figure 2. *Cont.*

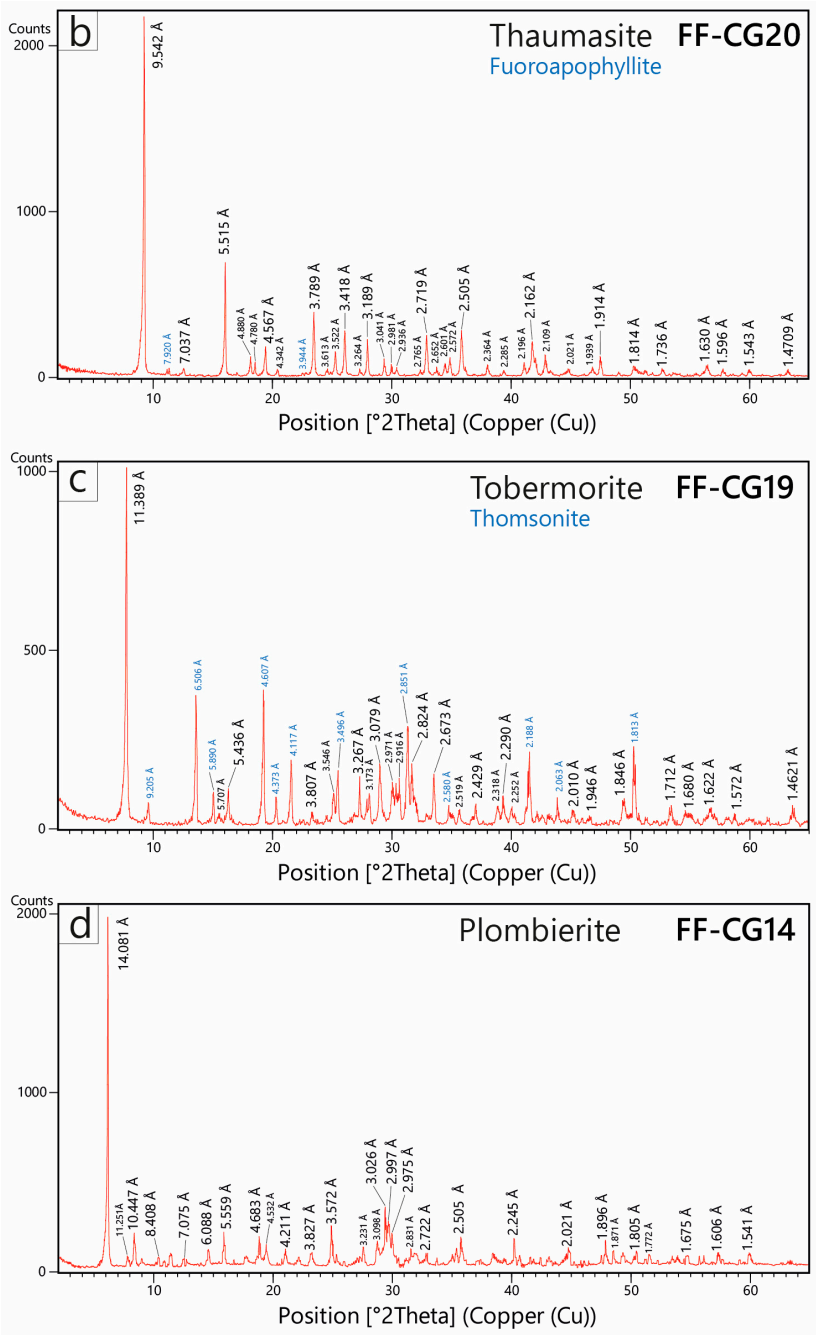

Figure 2. XRD patterns of the natural C-S-H minerals from the Grolla quarry, with the indication of D-spacing. (**a**) Xonotlite with minor calcite (FF-CF13); (**b**) thaumasite with minor fluoroapophyllite (FF-CG20); (**c**) Tobermorite with subordinate thomsonite from (FF-CG19); (**d**) plombierite (FF-CG14). The d-spacing values of minor minerals are in blue.

The chemical analysis of xonotlite from Grolla quarry shows a composition close to its ideal formula (Table 2). It is a hydrated calcium silicate, with 49.24–50.44 wt% SiO_2 and 46.66–48.13 wt% CaO. Other elements, such as Al_2O_3, FeO, and MgO, are only present in trace amounts, and no significant variations in composition were observed across the different crystal forms.

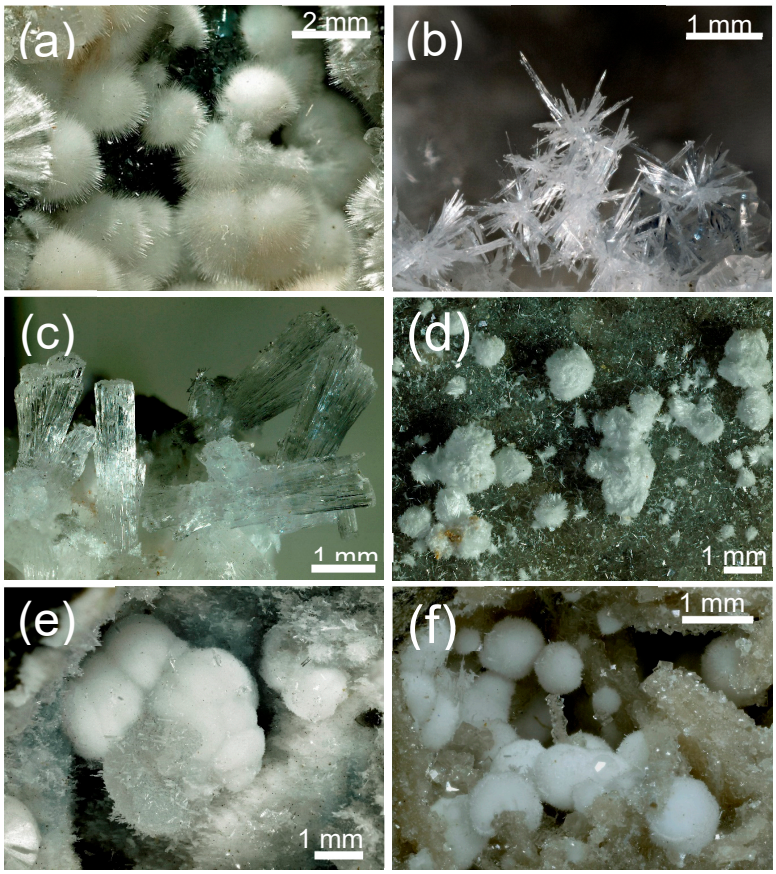

Figure 3. (**a**) Fibrous xonotlite crystals grouped in millimetric silky-looking spheroidal to botryoidal clusters (CG11); (**b**) needle-like xonotlite crystals grouped into silky, fibrous clusters (CG13); (**c**) prismatic vitreous crystals of thaumasite with a pseudo-hexagonal section (CG20); (**d**) tobermorite in sub-spherical, fibrous-radial forms creating white, silky, botryoidal aggregates (CG19); (**e**,**f**) plombierite in white botryoidal aggregates with a silky sheen, formed by small, sub-spherical fibrous-radial crystals (CG19).

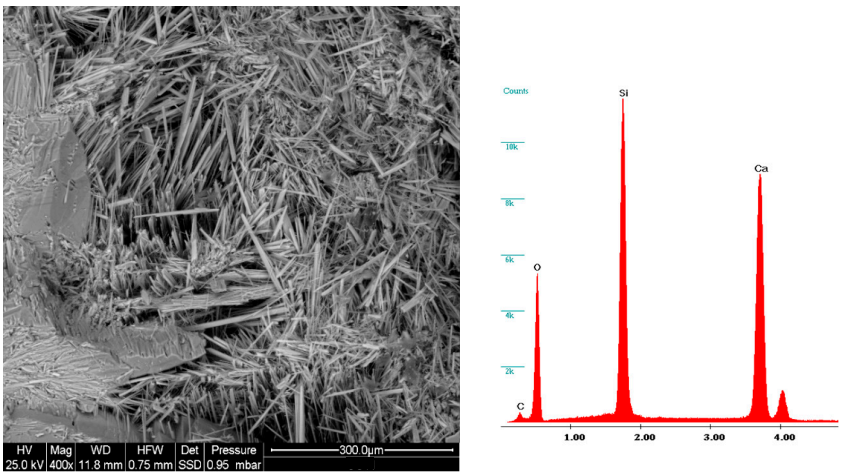

Figure 4. Typical morphologies of xonotlite crystals from the Grolla quarry. The crystals vary from flattened prismatic shapes to highly elongated acicular forms, with some developing into strongly fibrous structures. The co-growth of xonotlite with fluoroapophyllite crystals is visible, with fluoroapophyllite appearing in the left part of the image.

4.2. Thaumasite $Ca_3Si(OH)_6(CO)_3(SO_4)\cdot 12H_2O$

Thaumasite is a rare, naturally occurring mineral discovered in 1878 by Baron von Nordenskiöld at the Areskuta copper mine in Sweden. Its name comes from the Greek word thaumazein, meaning "to be surprised", due to its unusual composition, which includes carbonate, sulfate, and hexahydrosilicate groups. A very particular crystal chemical formula characterizes thaumasite: it contains ~42% H_2O, 7% CO_2, 13% SO_3, 28% CaO, and 10% SiO_2, giving it a very low density (~1.89 g/cm^3). Thaumasite formation requires a source of these ions. The crystal-chemical structure of thaumasite was solved only recently (late 1900s) through X-ray diffraction analysis of single crystals [42–44]. It consists of columns of $[Ca_3Si(OH)_6(H_2O)_{12}]^{4+}$ parallel to [001] and linked to CO_3^{2-} and SO_4^{2-} groups and water molecules via hydrogen bonds. Thaumasite is the only known mineral with silicon in six-fold coordination with hydroxyl groups (OH) under low-pressure conditions [45,46]. Thaumasite belongs to the ettringite group and forms a secondary phase at low temperatures in mafic igneous and metamorphic rocks. It is often found alongside minerals like ettringite, zeolites, calcite, gypsum, and tobermorite. In concrete, thaumasite is significant due to its role in sulfate attack, where sulfate ions react with cement compounds (C-S-H, portlandite) to form gypsum, ettringite, or thaumasite [47–50]. These reactions degrade concrete in sulfate-rich environments.

Thaumasite in the Grolla quarry is typically found in small, fibrous to acicular crystals or prismatic shapes with a hexagonal section (Figure 3c). The more common forms are fibrous-radial aggregates, whitish in color, forming sub-spherical or botryoidal shapes, and chaotic clusters of acicular crystals, transparent to translucent, forming fan-like or intertwined aggregates, especially with calcite, barite, and fluorapophyllite crystals (Figure 5). Microscopic observations show that thaumasite is one of the first minerals to crystallize on cavity and vesicle walls, along with calcite and fluoroapophyllite. Less commonly, thaumasite can form thin, whitish patinas or crusts with a silky sheen, often hard to distinguish from minerals like xonotlite or plombierite without detailed analysis.

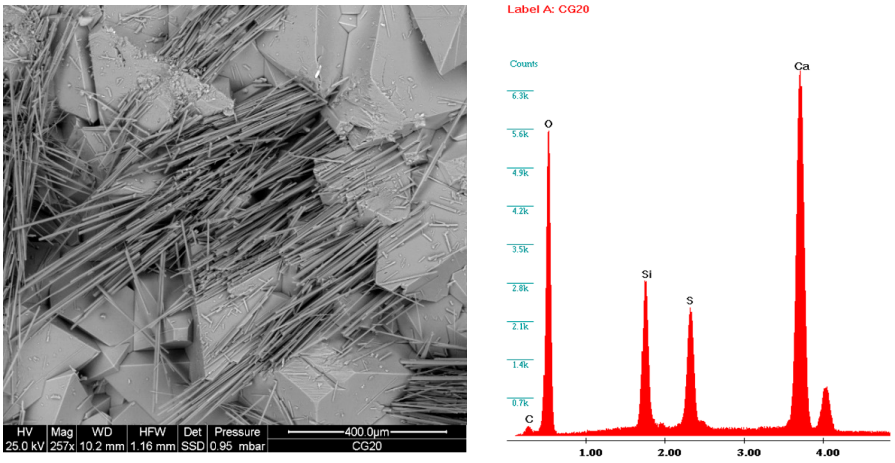

Figure 5. Thaumasite crystals associated with fluoroapophyllite from the Grolla quarry exhibit a very elongated prismatic to acicular habit, indicating their fibrous nature and growth patterns. The EDS spectrum is related to thaumasite crystals, with the typical chemical composition given by silicon, calcium, carbon, and sulfur.

Thaumasite from the Grolla quarry is chemically consistent (Table 2). Calcium is always the most abundant cation (CaO ~26–27 wt%), while SiO_2 is in the order of 10 wt%. The SO_3 group is present in significant quantities (12–13 wt%), as is CO_2 (7–8 wt%). The H_2O content is between 42 and 43 wt%, and the halogen (F, Cl) content is less than 1%, as is that of phosphorus and iron.

4.3. Tobermorite (Tobermorite-11 Å) $Ca_5Si_6O_{17}$ $5H_2O$

Tobermorite was first identified by Heddle in 1880 in samples from several locations in Scotland, especially near Tobermory on the Isle of Mull [51]. X-ray diffraction studies confirmed its status as a distinct mineral in the mid-20th century, revealing a characteristic basal reflection at 11.3 Å [52–54]. Significant progress has been made in understanding the structure of minerals in the tobermorite group over the past few decades. Studies by Merlino et al. [55,56] and Bonaccorsi et al. [57] have determined their crystal structures, providing insights into this group's chemical and structural differences.

The minerals in the tobermorite group are hydrated calcium silicates similar to the crystalline phases (C-S-H) formed during cement hydration. Structurally, tobermorites consist of layers of calcium polyhedra (with seven-fold coordination) arranged parallel to the (001) plane [11]. These layers are connected to single chains of "wollastonite-type" tetrahedra on both sides. Their classification is based on water content, which affects the spacing between layers (basal distance) and, thus, their structure. Three types of tobermorites were named based on hydration levels: plombierite (highly hydrated, 14 Å basal distance), tobermorite (moderately hydrated, 11 Å basal distance), and riversideite (low hydration, 9 Å basal distance). Recently, advances in understanding their crystal chemistry have led to a standardized naming system and the creation of the Tobermorite Supergroup, named after the most common mineral in this category [11,58]. According to IMA (International Mineralogical Association), the Tobermorite Supergroup includes tobermorite group minerals (obermorite and kenotobermorite), clinotobermorite group minerals (clinotobermorite, kenoclinotobermorite, and kalitobermorite), and two additional minerals (plombierite and riversideite). Although plombierite and riversideite are not officially recognized names, they are widely used in the scientific literature and considered reference species [58].

Recent research has clarified tobermorite's crystal chemistry and thermal behavior [59,60]. Its calcium content varies between 4 and 5 atoms per formula unit (apfu). Lower calcium levels may result from non-homogeneous material or calcium-poor phases, while higher levels may occur due to associations with calcium-rich phases like xonotlite or calcite. Aluminum can also replace silicon in the structure, reaching up to 1 apfu, though aluminum-free samples are rare and found mainly in South Africa's Kalahari Manganese Field [61]. Tobermorite mixes two end-member compositions: $Ca_4Si_6O_{15}(OH)_2{\cdot}5H_2O$ and $Ca_5Si_6O_{17}{\cdot}5H_2O$. The slight difference in composition influences its thermal behavior: a higher calcium content corresponds to "normal" thermal behavior, while low-Ca samples behave "anomalously" [60].

In the samples from the Grolla quarry, the tobermorite appears in several forms. It can form as (1) colorless needle-like crystals, transparent to translucent, often in fibrous-radial aggregates; (2) whitish fibrous crystals exhibiting pseudo-radial growth or small bundles (Figure 6a); (3) sub-spherical, fibrous-radial forms creating small, silky, botryoidal aggregates (Figure 3d); (4) intertwined needle-like crystals forming chaotic aggregates; and (5) thin coatings or vein fillings, appearing fine-grained, whitish, and silky to earthy in luster. Like thaumasite, microscopic evidence suggests that tobermorite also forms during the early stages of crystallization in mineralized cavities.

The chemical composition of Grolla quarry tobermorite is uniform and matches its theoretical formula (Table 2). It contains ~45 wt% SiO_2, 34–35 wt% CaO (4–5 apfu), and low aluminum (<1 wt% Al_2O_3), indicating minimal silicon–aluminum substitution. Its water content ranges between 19 and 21 wt%.

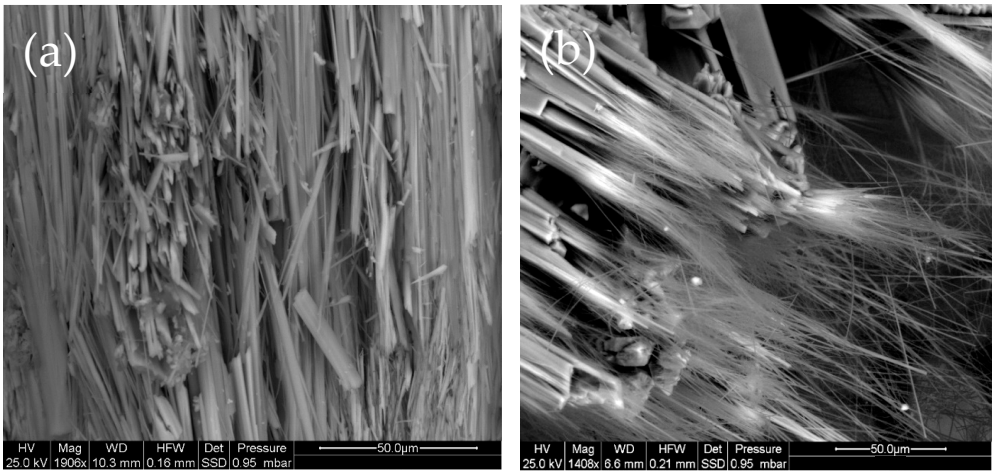

Figure 6. (**a**) Prismatic to fibrous crystals of tobermorite forming small bundles; (**b**) prismatic-acicular crystals of plombierite displaying a striking extremely fibrous termination, reflecting their characteristic morphology.

4.4. Plombièrite (Tobermorite-14 Å) $Ca_5Si_6O_{16}(OH)_2$ $7H_2O$

Plombierite belongs to the Tobermorite Supergroup, as noted in the nomenclature guidelines of the CNMNC (Commission on New Minerals, Nomenclature and Classification) and the IMA (International Mineralogical Association). While minerals in the tobermorite and clinotobermorite groups are officially recognized, plombierite and riversideite are not fully acknowledged. Still, they are considered reference species due to their established use in the scientific literature.

Plombierite was first used in 1858 to describe a silicate gel formed by thermal waters in Roman-era cementitious materials in Plombières, France [62]. In the mid-1900s, McConnell analyzed a similar material from Ballycraigy, Ireland, using X-ray diffraction [52]. The material was identified as a hydrated calcium silicate (C-S-H) group member, with the most hydrated phase classified as plombierite. It was later found that plombierite is a variety of tobermorite with a basal spacing of 14 Å, now known as tobermorite-14 Å. Despite this, the name plombierite remains widely used.

The structure of plombierite has been solved using a specimen from Crestmore (California, USA) [57]. Like other hydrated calcium silicates, plombierite consists of layers of calcium polyhedra (CaO_7) parallel to (001). These layers are linked by single tetrahedra (SiO_4) chains, arranged along the b-axis, and stacked along the c-axis. The layers are connected by extra calcium ions and water molecules, which fill cavities in the structure. The water content of plombierite determines its basal spacing, giving it the highest hydration level among the phases in the Tobermorite Supergroup, with a basal distance of 14 Å [60,63]. In this structure, the layers are separated by calcium ions and nearly double the water molecules found in the less hydrated 11 Å phases (five water molecules versus three). Concerning the ideal chemical formula, the composition of plombierite shows limited variability, with minor changes in the calcium content (usually 4.5–5 atoms per formula unit) and small aluminum–silicon substitutions.

In the Grolla quarry, plombierite generally appears as colorless needle-like crystals, transparent to translucent, often forming fibrous-radial aggregates (Figure 3e,f), or whitish acicular crystals, sometimes in pseudo-radial clusters or small bundles displaying striking extremely fibrous termination (Figure 6b). More frequently, plombierite forms botryoidal aggregates with a silky sheen, formed by small, sub-spherical fibrous-radial crystals, or it can be found as thin coatings or vein fillings, fine-grained with a silky to earthy luster, and whitish in color. Plombierite forms later than other minerals in all observed samples and often appears at the ends of tobermorite crystals.

Plombierite from the Grolla quarry shows slight variability across samples, and two main groups can be distinguished based on the major element composition (Table 2). The first group shows slightly higher silica (SiO_2 43–44 wt%) and lower calcium (CaO 30–33 wt%) and aluminum (Al_2O_3 0.1–0.2 wt%) contents, while in the second group, silica varies from 41 to 42 wt%, calcium is in the range 33–34 wt% and aluminum is more than 1 wt%. The water content in all the samples ranges between 19wt% and 21wt%.

4.5. Origin of C-S-H Minerals and Potential Implications

Natural C-S-H minerals typically form through heat-driven metamorphic reactions in contact zones between silicate and carbonate rocks [63,64]. Recent research highlights significant carbonation reactions in calcium silicate hydrate-bearing rocks [13,65]. These reactions generally occur in low-temperature hydrated calcium and aluminum silicate minerals surrounding high-temperature metamorphic calcium or aluminum silicate cores. Basic and ultrabasic magmas, rich in calcium, magnesium, and iron silicates like olivine, serpentine, pyroxene, and plagioclase, are especially reactive with dissolved CO_2 in water, making them well suited for forming solid carbonates [66–68]. Unfortunately, the data collected from the investigated samples do not allow for the reconstruction of a precise genetic crystallization sequence of the C-S-H minerals, as additional information is required. However, based on the data and observations of the samples and their growth conditions, an early crystallization phase of C-S-H minerals at the Grolla quarry, possibly linked to high-temperature metasomatic events, can be proposed. These events can occur in the contact zones between basic and ultrabasic melts associated with the magmatism of the Veneto Volcanic Province and the surrounding carbonate rocks. Thaumasite and tobermorite likely crystallized during this phase, along with calcite and fluorapophyllite. Later, a lower-temperature phase, possibly linked to hydrothermal processes that have already been widely described in this area [25], could have led to the formation of xonotlite and plombierite, along with sulfates (e.g., baryte) and zeolites such as chabazite, phillipsite/harmotome, natrolite, and thomsonite.

Finally, a final consideration emerges from the discovery, in the Grolla quarry samples, of C-S-H minerals with an extremely fibrous appearance. These characteristics raise worries about potential adverse health effects. Small particles, especially those with a fibrous shape, are known to cause toxic and cancerous lung effects [69–72]. Most scientific knowledge about the toxicity and cancer-causing effects of fibrous particles comes from research on asbestos, the most extensively studied mineral fiber. However, recent studies on erionite and other fibrous zeolites have grown significantly, providing new insights into the toxicology of fibrous particles [73–75]. The presence of fibrous minerals is particularly relevant for carbonate and volcanic rocks, which are widely mined and processed in the same quarries, with the finished products distributed for various uses. The discovery of C-S-H minerals with a highly fibrous habit in the Lessini Mountains suggests the need for future studies to quantify potentially airborne fibers for a preliminary risk assessment.

5. Concluding Remarks

This study provides a comprehensive analysis of natural calcium silicate hydrates (C-S-H) from the Grolla quarry in the Lessini Mountains of Northern Italy. The main conclusions are as follows:

- The minerals identified at the Grolla quarry are predominantly silicates, with subordinate carbonates and sulfates. The most common silicates are zeolites, including chabazite, phillipsite/harmotome, natrolite, and thomsonite, often associated with calcite, fluoroapophyllite, and barite.

- Unlike other mineralized areas in the Lessini Mountains, the Grolla quarry uniquely yields calcium silicate hydrate minerals (C-S-H) such as thomsonite, xonotlite, tobermorite, and plombierite. Most of the C-S-H minerals exhibit an acicular to extremely fibrous habit.
- The origin of the main phases in the Grolla quarry can be linked to metasomatic events and hydrothermal stages. This site offers a unique opportunity to study complex crystalline overgrowths and the specific crystal chemistry of rare natural mineral phases, such as C-S-H minerals.
- Finally, the presence of C-S-H phases with a highly fibrous structure raises concerns for human health, especially given the number of quarries and mining activities in the Lessini Mountains.

Author Contributions: M.M.: supervision, conceptualization, investigation, data curation, writing—original draft preparation, writing—review and editing, and funding acquisition. M.G.: formal analysis, data curation, and writing—review and editing. F.F.: sample collection, data curation, and writing—review and editing. All authors have read and agreed to the published version of the manuscript.

Funding: This research was conducted under the framework of the 2022 research programs of the Department of Pure and Applied Sciences of the University of Urbino Carlo Bo (project "New asbestiform natural fibers: mineralogical and physical-chemical characterization of fibrous zeolites", responsible M. Mattioli).

Data Availability Statement: Data are contained within the article. The data presented in this study can be seen in the content above.

Conflicts of Interest: The authors declare no conflicts of interest. The funders had no role in the study's design, in the collection, analyses, or interpretation of the data, in the writing of the manuscript, or in the decision to publish the results.

References

1. Scrivener, K.L.; Kirkpatrick, R.J. Innovation in use and research on cementitious material. *Cem. Concr. Res.* **2008**, *38*, 128–136. [CrossRef]
2. Richardson, I.G.; Groves, G.W. Models for the composition and structure of calcium silicate hydrate (C-S-H) gel in hardened tricalcium silicate pastes. *Cem. Concr. Res.* **1992**, *22*, 1001–1010. [CrossRef]
3. Richardson, I.G. The nature of C-S-H in hardened cements. *Cem. Concr. Res.* **1999**, *29*, 1131–1147. [CrossRef]
4. Richardson, I.G. The calcium silicate hydrates. *Cem. Concr. Res.* **2008**, *38*, 137–158. [CrossRef]
5. Picker, A.; Nicoleau, L.; Burghard, Z.; Bill, J.; Zlotnikov, I.; Labbez, C.; Nonat, A.; Cölfen, H. Mesocrystalline calcium silicate hydrate: A bioinspired route toward elastic concrete materials. *Sci. Adv.* **2017**, *3*, e1701216. [CrossRef]
6. Tang, S.; Wang, Y.; Geng, Z.; Xu, X.; Yu, W.; A, H.; Chen, J. Structure, Fractality, Mechanics and Durability of Calcium Silicate Hydrates. *Fractal Fract.* **2021**, *5*, 47. [CrossRef]
7. Faucon, P.; Petit, J.C.; Charpentier, T.; Jacquinot, J.F.; Adenot, F. Silicon substitution for aluminum in calcium silicate hydrates. *J. Am. Ceram. Soc.* **1999**, *82*, 1307–1312. [CrossRef]
8. Hou, D.; Zhao, T.; Ma, H.; Li, Z. Reactive molecular simulation on water confined in the nanopores of the valcium silicate hydrate gel: Structure, reactivity, and mechanical properties. *J. Phys. Chem. C* **2015**, *119*, 1346–1358. [CrossRef]
9. Papatzani, S.; Paine, K.; Calabria-Holley, J. A comprehensive review of the models on the nanostructure of calcium silicate hydrates. *Constr. Build. Mater.* **2015**, *74*, 219–234. [CrossRef]
10. Jakobsson, S.; Moore, J.G. Hydrothermal minerals and alteration rates at Surtsey volcano, Iceland. *Geol. Soc. Am. Bull.* **1986**, *97*, 648–659. [CrossRef]
11. Bonaccorsi, E.; Merlino, S. Modular microporous minerals: Cancrinite-davyne group and CSH phases. *Rev. Mineral. Geochem.* **2005**, *57*, 241–290. [CrossRef]
12. Milodowski, A.E.; Rochelle, C.A.; Lacinska, A.; Wagner, D. A natural analogue study of CO_2-cement interaction: Carbonation of calcium silicate hydrate-bearing rocks from Northern Ireland. *Energy Procedia* **2011**, *4*, 5235–5242. [CrossRef]
13. Marincea, S.; Bilal, E.; Verkaeren, J.; Pascal, M.L.; Fonteilles, M. Superposed parageneses in the spurrite-, tilleyite and gehlenite-bearing skarns from Cornet Hill, Apuseni Mountains, Romania. *Can. Mineral.* **2001**, *39*, 1435–1453. [CrossRef]

14. Hoffmann, C.; Armbruster, T. Clinotobermorite, $Ca_5[Si_3O_8(OH)]_2 \cdot 4H_2O$–$Ca_5[Si_6O17] \cdot 5H_2O$, a natural C-S-H(I) type cement mineral: Determination of the substructure. *Z Kristallogr.* **1997**, *212*, 864–873. [CrossRef]
15. Aguirre, L.; Dominguez-Bella, S.; Morata, D.; Wittke, O. An occurrence of tobermorite in tertiary basalts from Patagonia, Chile. *Can. Mineral.* **1998**, *36*, 1149–1155.
16. Maeshima, T.; Noma, H.; Sakiyama, M.; Mitsuda, T. Natural 1.1 and 1.4 nm tobermorites from Fuka, Okayama, Japan: Chemical analysis, cell dimensions, 29Si NMR and thermal behavior. *Cem. Concr. Res.* **2003**, *33*, 1515–1523. [CrossRef]
17. Hu, S.; Xu, Z.; Ma, X.; Huo, Y.; Yang, Y. Preparation of C-S-H seeds from solid waste and its application as Portland cement accelerator. *Constr. Build. Mater.* **2024**, *428*, 136277. [CrossRef]
18. Zampieri, D. Segmentation and linkage of the Lessini Mountains normal Faults, Southern Alps, Italy. *Tectonophys.* **2000**, *319*, 19–31. [CrossRef]
19. De Vecchi, G.P.; Gregnanin, A.; Piccirillo, E.M. Aspetti petrogenetici del vulcanesimo terziario veneto. *Mem. Ist. Geol. Mineral. Dell'universita Padova* **1976**, *30*, 1–32.
20. Barbieri, G.; De Zanche, V.; Medizza, F.; Sedea, R. Considerazioni sul vulcanismo terziario del Veneto occidentale e del Trentino meridionale. *Rend. Soc. Geol. Ital.* **1982**, *4*, 267–270.
21. De Vecchi, G.P.; Sedea, R. The Paleogene basalt ofthe Veneto region (NE Italy). *Mem. Ist. Geol. Mineral. Dell'università Padova* **1995**, *47*, 253–274.
22. Milani, L.; Beccaluva, L.; Coltorti, M. Petrogenesis andevolution of the Euganean magmatic complex, Veneto Region, North-East Italy. *Eur. J. Mineral.* **1999**, *11*, 379–399. [CrossRef]
23. Bonadiman, C.; Coltorti, M.; Milani, L.; Salvini, L.; Siena, F.; Tassinari, R. Metasomatism in the lithospheric mantleand its relationships to magmatism in the Veneto Volcanic Province, Italy. *Period. Di Mineral.* **2001**, *70*, 333–357.
24. Beccaluva, L.; Bianchini, G.; Bonadiman, C.; Coltorti, M.; Milani, L.; Salvini, L.; Siena, F.; Tassinari, R. Intraplate litospheric and sublitospheric components in the Adriatic domain: Nephelinite to tholeiite magma generation in the Paleogene Veneto volcanic province, southern Alps. *Mineral. Soc. Am. Spec. Pap.* **2007**, *418*, 131–152.
25. Mattioli, M.; Cenni, M.; Passaglia, E. Secondary mineral assemblages as indicators of multi stage alteration processes in basaltic lava flows: Evidence from the Lessini Mountains, Veneto Volcanic Province, Northern Italy. *Period. Mineral.* **2016**, *85*, 1–24.
26. Mattioli, M.; Cenni, M. First Occurrence of Willhendersonite in the Lessini Mounts, Northern Italy. *Crystals* **2021**, *11*, 109. [CrossRef]
27. Cametti, G.; Giordani, M. Humidity-and temperature-dependent study of YUG type zeolite. A new dehydrated topology. *Microporous Mesoporous Mater.* **2024**, *363*, 112811. [CrossRef]
28. Giordani, M.; Mattioli, M.; Dogan, M.; Dogan, A.U. Potential carcinogenic erionite from Lessini Mounts, NE Italy: Morphological, mineralogical and chemical characterization. *J. Toxicol. Environ. Health A* **2016**, *79*, 808–824. [CrossRef]
29. Giordani, M.; Mattioli, M.; Ballirano, P.; Pacella, P.; Cenni, M.; Boscardin, M.; Valentini, L. Geological occurrence, mineralogical characterization and risk assessment of potentially carcinogenic erionite in Italy. *J. Toxicol. Environ. Health B* **2017**, *20*, 81–103. [CrossRef]
30. Cangiotti, M.; Battistelli, M.; Salucci, S.; Falcieri, E.; Mattioli, M.; Giordani, M.; Ottaviani, M.F. Electron paramagnetic resonance and transmission electron microscopy study of the interactions between asbestiform zeolite fibers and model membranes. *J. Toxicol. Environ. Health A* **2017**, *80*, 171–187. [CrossRef] [PubMed]
31. Mattioli, M.; Giordani, M.; Arcangeli, P.; Valentini, L.; Boscardin, M.; Pacella, A.; Ballirano, P. Prismatic to asbestiform offretite from Northern Italy: Occurrence, morphology and crystal-chemistry of a new potentially hazardous zeolite. *Minerals* **2018**, *8*, 69. [CrossRef]
32. Giordani, M.; Ballirano, P.; Pacella, A.; Meli, M.A.; Roselli, C.; Di Lorenzo, F.; Fagiolino, I.; Mattioli, M. Fibrous mordenite from Northern Italy: Another potentially hazardous zeolite. *Minerals* **2022**, *121*, 627. [CrossRef]
33. Giordani, M.; Cametti, G.; Di Lorenzo, F.; Churakov, S.V. Real-time observation of fibrous zeolites reactivity in contact with simulated lung fluids (SLFs) obtained by atomic force microscope (AFM). *Minerals* **2019**, *9*, 83. [CrossRef]
34. Goldstein, J.I.; Newbury, D.E.; Echlin, P.; Joy, D.C.; Romig, A.D.; Lyman, C.E.; Fiori, C.; Lifshin, E. *Scanning Electron Microscopy and X-Ray Microanalysis*, 2nd ed.; Plenum Press: New York, NY, USA, 1992.
35. Pacella, A.; Ballirano, P.; Cametti, G. Quantitative chemical analysis of erionite fibres using a micro-analytical SEM-EDX method. *Eur. J. Mineral.* **2016**, *28*, 257–264. [CrossRef]
36. Rammelsberg, C. Über den Xonaltit, ein neues wasserhaltiges Kalksilikat, und den Bustamit aus Mexico. *Z. Deutsch. Geol. Ges.* **1866**, *18*, 33–34.
37. O'brien, J.P.; Rodgers, K.A. Xonotlite and rodingites from Wairere, New Zealand. *Mineral. Mag.* **1973**, *39*, 233–240. [CrossRef]
38. Kalousek, G.L.; Mitsuda, T.; Taylor, H.F.W. Xonotlite: Cell parameters, thermogravimetry and analytical electron microscopy. *Cem. Concr. Res.* **1977**, *7*, 305–312. [CrossRef]
39. Churakov, S.V.; Mandaliev, P. Structure of the hydrogen bonds and silica defects in the tetrahedral double chain of xonotlite. *Cem. Concr. Res.* **2008**, *38*, 300–311. [CrossRef]

40. Hejny, C.; Armbruster, T. Polytypism in xonotlite $Ca_6Si6O_{17}(OH)_2$. *Z. Für Krist. Cryst. Mater.* **2001**, *216*, 396–408. [CrossRef]
41. Bernstein, S.; Fehr, K.T.; Hochleitner, R. Crystal chemistry of Xonotlite Ca6Si6O17(OH)2. Part I: Determination of polytypes using X-Ray Powder Diffraction (XRPD). *N. Jb. Miner. Abh.* **2009**, *186*, 153–162. [CrossRef]
42. Hurlbut, C.S.J.; Baum, J.L. Ettringite from Franklin, New Jersey. *Am. Mineral.* **1960**, *45*, 1137–1143.
43. Knill, D.C. Thaumasite from Co. Down, Northern Ireland. *Mineral. Mag. J. Mineral. Soc.* **1960**, *32*, 416–418. [CrossRef]
44. Edge, R.A.; Taylor, H.F.W. Crystal structure of thaumasite [Ca_3Si (OH) 6.12 H_2O](SO_4)(CO_3). *Acta Crystallogr. Sect. B Struct. Crystallogr. Cryst. Chem.* **1971**, *27*, 594–601. [CrossRef]
45. Duffy, J.A.; Macphee, D.E. The Coordination Number of Silicon in Silicon-Oxygen Compounds: The Special Case of 6-Fold Coordination in Thaumasite. *J. Phys. Chem. B* **2007**, *111*, 8740–8745. [CrossRef]
46. Scholtzová, E.; Kucková, L.; Kožíšek, J.; Pálková, H.; Tunega, D. Experimental and computational study of thaumasite structure. *Cem. Concr. Res.* **2014**, *59*, 66–72. [CrossRef]
47. Crammond, N. The occurrence of thaumasite in modern construction—A review. *Cem. Concr. Compos.* **2002**, *24*, 393–402. [CrossRef]
48. Crammond, N.J. The thaumasite sulfate attack in the UK. *Cem. Concr. Compos.* **2003**, *25*, 809–818. [CrossRef]
49. Tsivilis, S.; Sotiriadis, K.; Skaropoulou, A. Thaumasite sulfate attack (TSA) in limestone cement pastes. *J. Eur. Ceram. Soc.* **2007**, *27*, 1711–1714. [CrossRef]
50. Rahman, M.M.; Bassuoni, M.T. Thaumasite sulfate attack on concrete: Mechanisms, influential factors and mitigation. *Constr. Build. Mater.* **2014**, *73*, 652–662. [CrossRef]
51. Heddle, M.F. Preliminary notice of substances which may prove to be new minerals. *Mineral. Mag.* **1880**, *4*, 117–123. [CrossRef]
52. McConnell, J.D.C. The hydrated calcium silicates riversideite, tobermorite, and plombierite. *Mineral. Mag.* **1954**, *30*, 293–305. [CrossRef]
53. Megaw, H.D.; Kelsey, C.H. Crystal structure of tobermorite. *Nature* **1956**, *177*, 390–391. [CrossRef]
54. Hamid, S.A. The crystal structure of the 11Å natural tobermorite Ca2.25[Si3O7.5(OH)1.5] $1H_2O$. *Z. Für Krist. Cryst. Mater.* **1981**, *154*, 189–198. [CrossRef]
55. Merlino, S.; Bonaccorsi, E.; Armbruster, T. Tobermorites: Their real structure and OD character. *Amer. Mineral.* **1999**, *84*, 1613–1621. [CrossRef]
56. Merlino, S.; Bonaccorsi, E.; Armbruster, T. The real structure of tobermorite 11Å: Normal and anomalous forms, OD character and polytypic modifications. *Eur. J. Mineral.* **2001**, *13*, 577–590. [CrossRef]
57. Bonaccorsi, E.; Merlino, S.; Kampf, A.R. The Crystal Structure of Tobermorite 14 Å (Plombierite), a C–S–H Phase. *J. Am. Ceram. Soc.* **2005**, *88*, 505–512. [CrossRef]
58. Biagioni, C.; Merlino, S.; Bonaccorsi, E. The tobermorite supergroup: A new nomenclature. *Mineral. Mag.* **2015**, *79*, 485–495. [CrossRef]
59. Biagioni, C.; Bonaccorsi, E.; Merlino, S.; Bersani, D. New data on the thermal behavior of 14Å tobermorite. *Cem. Concr. Res.* **2013**, *49*, 48–54. [CrossRef]
60. Biagioni, C.; Bonaccorsi, E.; Lezzerini, M.; Merlino, S. Thermal behaviour of Al-rich tobermorite. *Eur. J. Mineral.* **2016**, *28*, 23–32. [CrossRef]
61. Biagioni, C.; Bonaccorsi, E.; Merlino, S.; Bersani, D.; Forte, C. Thermal behaviour of tobermorite from N'Chwaning II mine (Kalahari Manganese Field, Republic of South Africa) II. Crystallographic and spectroscopic study of tobermorite 10 Å. *Eur. J. Mineral.* **2012**, *24*, 991–1004. [CrossRef]
62. Daubrée, M. Mémoire sur le relation des sources thermals de Plombières avec le filons métalliféres er sur la formation contemporaine des zéolithes. *Ann. Min.* **1858**, *13*, 227–256.
63. Constantinescu, E.; Ilinca, G.; Ilinca, A. Contributions to the study of the Oravita–Ciclora skarn occurrence, southwestern Banat. D.S. *Inst. Geol. Geofiz. 2 Zăcăminte* **1988**, *72*, 27–45.
64. Stoppa, F.; Scordari, F.; Mesto, E.; Sharygin, V.; Bortolozzi, G. Calcium-aluminum-silicate-hydrate "cement" phases and rare Ca-zeolite association at Colle Fabbri, Central Italy. *Open Geosci.* **2010**, *2*, 175–187. [CrossRef]
65. Zhang, Y.Q.; Radha, A.V.; Navrotsky, A. Thermochemistry of two calcium silicate carbonate minerals: Scawtite, $Ca7(Si_6O_{18})(CO_3)\cdot 2H_2O$, and spurrite, $Ca_5(SiO_4)_2(CO_3)$. *Geochim. Cosmochim. Acta* **2013**, *115*, 92–99. [CrossRef]
66. Ferrini, V.; De Vito, C.; Mignardi, S. Synthesis of nesquehonite by reaction of gaseous CO_2 with Mg chloride solution: Its potential role in the sequestration of carbon dioxide. *J. Hazard. Mater.* **2009**, *168*, 832–837. [CrossRef] [PubMed]
67. Matter, J.M.; Kelemen, P.B. Permanent storage of carbon dioxide in geological reservoirs by mineral carbonation. *Nat. Geosci.* **2009**, *2*, 837–841. [CrossRef]
68. Orr, F.M.J. CO_2 capture and storage: Are we ready? *Energy Environ. Sci.* **2009**, *2*, 449–458. [CrossRef]
69. Stanton, M.F.; Layard, M.; Tegeris, A.; Miller, E.; May, M.; Morgan, E.; Smith, A. Relation of particle dimension to carcinogenicity in amphibole asbestoses and other fibrous minerals. *J. Natl. Cancer Inst.* **1981**, *67*, 965–975. [PubMed]
70. Fubini, B.; Fenoglio, I. Toxic potential of mineral dusts. *Elements* **2007**, *3*, 407–414. [CrossRef]

71. Aust, A.E.; Cook, P.M.; Dodson, R.D. Morphological and chemical mechanisms of elongated mineral particle toxicities. *J. Toxicol. Environ. Health Part B* **2011**, *14*, 40–75. [CrossRef]
72. Crovella, S.; Bianco, A.M.; Vuch, J.; Zupin, L.; Moura, R.R.; Trevisan, E.; Schneider, M.; Brollo, A.; Nicastro, E.M.; Cosenzi, A.; et al. Iron signature in asbestos-induced malignant pleural mesothelioma: A population-based autopsy study. *J. Toxicol. Environ. Health Part A* **2016**, *79*, 129–141. [CrossRef] [PubMed]
73. Giordani, M.; Mattioli, M.; Cangiotti, M.; Fattori, A.; Ottaviani, M.F.; Betti, M.; Ballirano, P.; Pacella, A.; Di Giuseppe, D.; Scognamiglio, V.; et al. Characterisation of potentially toxic natural fibrous zeolites by means of electron paramagnetic resonance spectroscopy and morphological-mineralogical studies. *Chemosphere* **2022**, *291*, 133067. [CrossRef] [PubMed]
74. Mattioli, M.; Giordani, M.; Dogan, M.; Cangiotti, M.; Avella, G.; Giorgi, R.; Dogan, A.U.; Ottaviani, M.F. Morpho-chemical characterization and surface properties of carcinogenic zeolite fibers. *J. Hazard. Mater.* **2016**, *306*, 140–148. [CrossRef] [PubMed]
75. Mattioli, M.; Ballirano, P.; Pacella, A.; Cangiotti, M.; Di Lorenzo, F.; Valentini, L.; Meli, M.A.; Roselli, C.; Fagiolino, I.; Giordani, M. Fibrous Ferrierite from Northern Italy: Mineralogical Characterization, Surface Properties, and Assessment of Potential Toxicity. *Minerals* **2022**, *12*, 626. [CrossRef]